Fire Exposure Modeling Considerations

An ioMosaic White Paper

Date: October 11, 2023
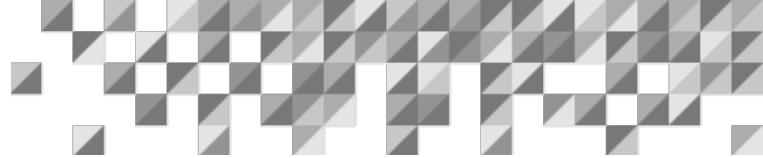
Introduction

A classic scenario in risk assessments is the exposure of process/storage vessels and piping to an external pool fire or a jet fire. The heat from a fire causes the temperature of the metal walls to increase and subsequent heat transfer from the metal walls causes the pressure and temperature of the vessel and piping contents to increase. The heating rate from fire exposure determines the pressure relief rate requirements for both boiling liquids and all-gas systems. Venting requirements can be estimated using, for example, the methods of API Standard 521 (2014) or the Design Institute for Emergency Relief Systems (DIERS) "Guidelines for Pressure Relief and Effluent Handling Systems" (2017).

For pressure vessels that are only protected from overpressure with pressure relief valves (PRVs), the PRVs continue to open and reseat at the PRV opening pressure and reseating pressure, respectively. As the metal wall temperature increases, the metal strength decreases. When vessels are exposed to fires for extended periods of time the metal wall will weaken enough to fail at the PRV reseat pressure. Thus PRVs cannot protect a vessel from an extended fire exposure if the actual wall stresses exceed the material strength (Melhem and Gaydos, 2015).

There is a substantial difference in the likelihood of vessel wall failure between vessels exposed to jet fires and those exposed to pool fires. Flame jet impingement causes localized high intensity heating. If the flame jet impinges on a dry vessel wall segment then wall failures can occur within a few minutes. Heating rates from pool fires depend on whether the vessel is total engulfed, partially engulfed, or heated from a distance by thermal radiation. In vessels containing liquids and exposed to pool fires, failures typically occur at the vapor/liquid interface because of increased thermal stress between the dry wall hot metal temperature and the wetted wall cooler metal temperature (Melhem and Gaydos, 2015).

Reasonable estimates of the estimated time to failure are an element of risk management (Melhem, 2021). A PRV can only be considered adequate for PRV overtemperature and overpressure protection when the estimated time to failure exceeds the fire duration. Also, the estimated time to failure is important for emergency response and risk analysis. The response time of risk mitigation measures must be less than the estimated time to failure to be effective. Finally, in the case of a fire, the emergency response team staging is influenced by knowing whether or not there is risk of vessel rupture.

In fire scenarios, the dynamic response of a pressure relief valve in vapor service depends upon transient heating effects of the vessel inventory. Fire heating of the vessel walls causes superheating of the vapor phase and thermal stratification of the liquid phase (Hendrickson, 2023). Consequences of these phenomena include more rapid pressurization and more frequent pressure relief valve cycling than is predicted using models based on thermodynamic equilibrium. These effects are considerations when evaluating pressure relief system performance.
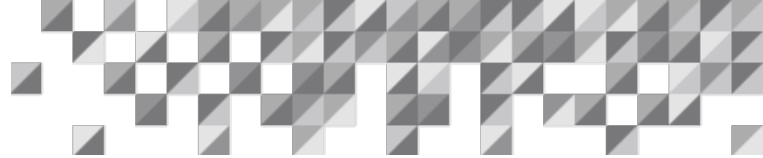
The cases considered in this paper were modeled using the commercial software package SuperChems™ provided by ioMosaic. SuperChems™ solves the time dependent material, momentum and energy balances along with thermodynamic equilibrium phase behavior. The model allows user input for fire parameters, such as flame temperature and emissivity, and the relevant heat transfer parameters. Vessel wall segmentation is provided to allow the user to specify which vessel wall segments are exposed to flames and hot gases. Model results include estimated time to failure and the estimated time to first relief.

2. Discussion

When a vessel containing liquid is first exposed to external fire, the radiative and convective heating of the vessel wall initially provides heat to the vessel inventory that is located in a thermal boundary layer near the vessel inside wall (Figure 2.1). With sufficient wall heating, boiling initially occurs in the thermal boundary layer while the bulk of the liquid inventory remains at or near its initial temperature. The boiling liquid in the thermal boundary layer rises to the top of the liquid inventory to form a saturated liquid layer. Thus the wall heating and boiling near the vessel wall results in liquid temperature stratification that influences the amount of liquid level rise. The liquid temperature stratification also causes a top-mounted pressure relief valve (PRV) to open earlier than it would if the mixture were well mixed at the average liquid temperature in the vessel.

Figure 2.1: Thermal and Hydraulic Processes during Fire Heating with Closed PRV
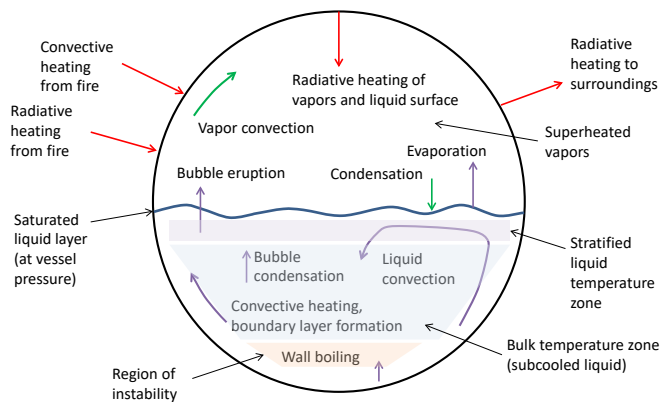
Temperature stratification also occurs in the vapor phase of the vessel inventory with the hottest temperatures near the vessel walls, resulting is a superheated vapor phase (Figure 2.1). Thus, before the PRD opens a superheated vapor phase is in contact with a saturated liquid layer located on top of the subcooled bulk liquid inventory. When the PRV first opens, the first fluid to be released is superheated vapor, thus the pressure decreases rapidly. As the superheated vapor is released, the vessel pressure decreases and liquid flashes from the saturated liquid layer. If the PRV blowdown is small enough, the preponderance of liquid flashing will be from the saturated liquid layer and the PRV will quickly reseat. If the PRV blowdown is large enough, the pressure can decrease enough to saturate the bulk liquid and also cause flashing to occur in it. In this case, it will take longer for the PRV to reseat, resulting in a longer PRV cycle time.
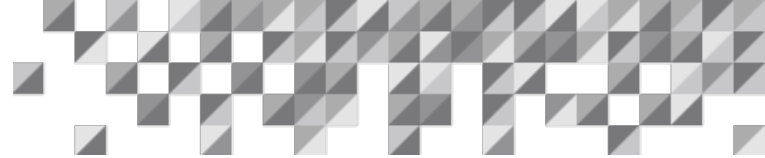
When a PRV opens, and flashing occurs in the bulk liquid there tends to be mixing of the liquid phase (Figure 2.2). This mixing decreases the temperature stratification and eventually saturation conditions are established throughout the liquid phase. Sustained vent flow does not occur until saturation conditions are established throughout the liquid phase. For a top-mounted PRV, flashing of the saturated liquid and flow of saturated vapors out through the PRV is sufficient to also saturate the vapor phase inventory.

Figure 2.2: Thermal and Hydraulic Processes during Fire Heating with Open PRV
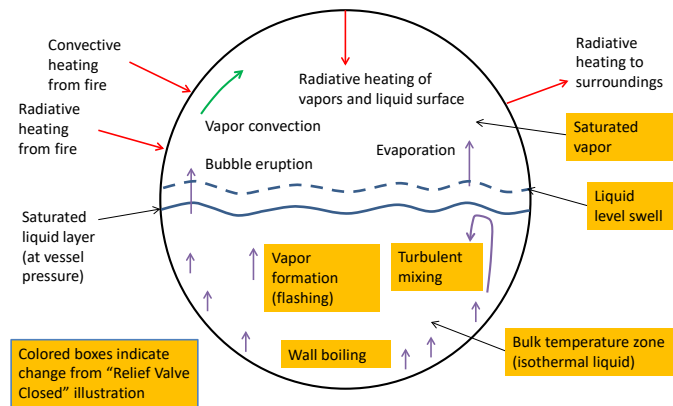
An example of liquid stratification, vapor superheating, and mixing effects are illustrated in Figure 2.3, from Birk, et.al (2003). The top temperature trace (lading 0) is located in the vapor space (90% vessel fill level) and the bottom temperature trace (lading 15) is located near the vessel bottom (10% vessel fill level). The vapor phase is heated to nearly 35°C hotter than the top surface of the liquid (lading 1) before the PRV first discharges at 140 seconds after the fire is initiated. Likewise, the top of the liquid phase (lading 1) is about 18°C hotter than the liquid near the bottom of the liquid phase when the PRV first opens. When the PRV begins to discharge, mixing occurs and the measured temperatures approach each other by about 220 seconds after fire exposure. However, in this case stratification and de-stratification continue to occur as the PRV cycles open and closed until the vessel ruptures 938 seconds after fire exposure.

The question arose regarding how much effect the temperature stratification and subsequent mixing have on the estimated time to first PRV discharge and the estimated time to vessel failure. The estimated time to first PRV discharge can be important if, for example, dynamic system load modeling is used to determine the hydraulic performance of effluent handling systems. Dynamic system load modeling during a common mode event, such as fire, is an established technique as described in API Standard 521 (2014). The estimated time to failure can be important, for example, when staging emergency response teams during a fire.
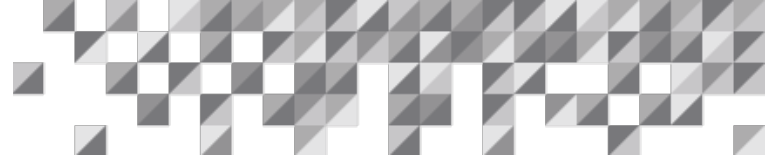
Figure 2.3: Liquid Temperature Stratification and Vapor Superheating (from Birk, et.al, 2003)
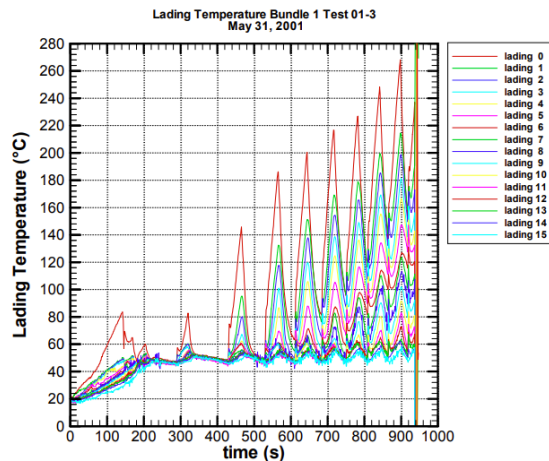
This report documents the results of efforts to model fire exposure of pressure vessels using Process Safety Office® SuperChems™ software by ioMosaic. SuperChems™ provides state of the art dynamic modeling capabilities of pressure relief scenarios. Important heat transfer parameters, such as fire temperature and vessel wall surface heat transfer coefficients are available as user inputs. The model was developed assuming thermodynamic equilibrium of the vapor and liquid phases. Thus deviation of the model results from experimental values is an indication of the importance of non-equilibrium phenomena, such as thermal stratification and vapor superheating. Note the scope of this study is relatively narrow. The systems studied only included the following:

- Wall heating by external fires (not bulk heating, e.g., heat of reaction)
- Churn-turbulent, non-reactive, non-viscous fluids (not bubbly, gassy or hybrid fluids)
- Vapor release through top mounted PRVs (not liquid releases)
- Only PRV performance was considered (not effluent handling system design)

Considerations for both the estimated time to first release and the estimated time to failure are discussed.

3. Case Studies

Four cases were modeled to test the predictions of a rigorous model, based on thermodynamic equilibrium, against experimental results. The fire exposure testing that was selected to model was that of Anderson et.al (1974), Birk et.al (2003), Melhem et.al (1993) and Moodie et.al (1988). For convenience, the experiments will be referred to by the name of the first author. Anderson and Moodie both totally engulfed the test vessels in pool fires while Melhem and Birk used propane torches to simulate pool fires. An overview of the test conditions is summarized in Table 3.1.
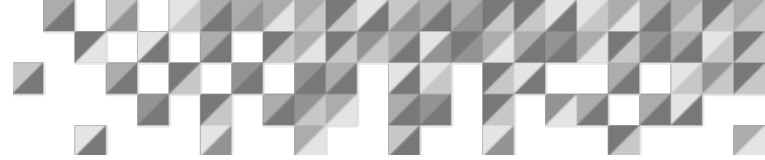
Table 3.1: Overview of Test Conditions

Test	Anderson	Birk	Melhem	Moodie
Vessel Description	33,600 gallon DOT 112A340W tank car	500 gallon (1890 liter) propane tanks	500 gallon (1890 liter) propane tanks	5 tonne LPG tank
Vessel Dimensions	10 ft. (3.05 m.) diameter x 60 ft. (18.29 m.) overall length	3 ft. (0.91 m.) diameter x 10 ft. (3.05 m.) overall length	3 ft. (0.91 m.) diameter x 10 ft. (3.05 m.) overall length	5.58 ft. (1.7 m.) diameter x 13.12 ft. (4 m.) overall length
Relief Valve	Midland A-3180-N	Fast opening ball valve (Note 2)	RegO pressure relief valve (Note 3)	Unspecified
Relief Valve Area	7.84 in^2 (50.6 cm^2)	21 mm nozzle diameter (0.537 in^2, 3.464 cm^2)	Nominal 1" (2.54 cm) diameter	1.375 in^2 (8.9 cm^2)
Vessel Contents	LPG	Commercial Propane	Commercial Propane	Commercial Propane
Vessel Initial Fill	96% (Note 1)	80%	40%	Variable: 22, 36, 58 and 72%
Fire Source	JP-4 jet fuel pool fire	Propane torches	Propane torches	Kerosene pool fire

Notes:
1. The initial fill level in the model was specified to be 78% to prevent the vessel from becoming liquid full.
2. The fast-opening ball valve was selected to achieve repeatable performance and was opened and closed at specified pressures by the control system. The set-up was modeled as a spring loaded PRV with the same opening and closing pressures.
3. Two cases were modeled in the Melhem tests, one with a PRV and one without a vent.

Some judgement is required when selecting parameters to model the fire and consequent radiation heat transfer. Generally speaking, literature values were selected for parameters such as surface emissivity and absorptivity and for the convective heat transfer coefficients. Where possible, the actual measured flame temperature was used as the heat source. The temperatures of the hot gases in contact with the vessel external walls were assumed to be equal to the flame temperatures since the fires totally engulfed the vessels, except in the cases of Birk and Melhem in which the flames were directed toward the vessel walls. Heat transfer parameters are summarized in Table 3.2.

When a vessel is exposed to and external fire, the combined radiative and convective heat transfer from the flame and hot gases to the vessel is given by the Stefan-Boltzmann equation.

$$Q = A\sigma F_{12}\left(\propto_{surface} \varepsilon_{flame} T_{flame}^4 - \varepsilon_{surface} T_{surface}^4\right) + Ah(T_{gas} - T_{surface})$$

Given that the heat transfer parameters are multiplied together, it is not possible to change the value of one variable without impacting the estimated value of other variables. The flames totally engulfed the vessels in the experiments of Anderson and Moodie, so the geometric view factor was set equal to 1.0 in both cases to reflect total engulfment of the vessels by the flames. The flame emissivity was set equal to 0.64 in the Anderson case based on the value reported by Anderson et.al (1974). The flame temperature was then set such that the calculated amount of fluid released equaled the measured value. The resulting flame temperature and heat flux were reasonably close to the measured values. As illustrated in Figure 3.1.
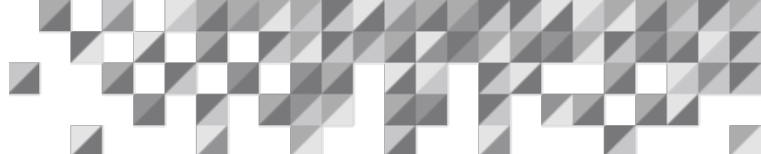
Table 3.2: Heat Transfer Parameters

Experiments	Anderson	Birk	Melhem	Moodie
Flame Properties				
Flame Emissivity	0.62	0.33	0.33	0.94
Flame Temperature, °F (K)	1526 (1103)	1880 (1300)	1880 (1300)	1251 (950)
Gas Temperature, °F (K)	1526 (1103)	1880 (1300)	1880 (1300)	1251 (950)
External Convective Heat Transfer Coefficient, BTU/ft^2 hr °F (W/m^2 K)	3.46 (20)	8.81 (50)	3.46 (20)	3.46 (20)
Geometric View Factor	1	0.01/1 (Note 1)	1	1
Atmospheric Transmissivity	1	1	1	1
Wall Properties				
Outer Surface Emissivity	0.9	0.9	0.9	0.8
Inner Surface Emissivity	0.8	0.66	0.66	0.8
Absorptivity	0.9	0.9	0.9	0.8
Wall/Vapor Heat Transfer Coefficient, BTU/ft^2 hr °F (W/m^2 K)	1.73 (10)	1.73 (10)	1.73 (10)	1.73 (10)
Wall/Liquid Heat Transfer Coefficient, BTU/ft^2 hr °F (W/m^2 K)	881 (5000)	881 (5000)	881 (5000)	881 (5000)
Wall/Condensing Film Heat Transfer Coefficient, BTU/ft^2 hr °F (W/m^2 K)	881 (5000)	881 (5000)	881 (5000)	881 (5000)
Vessel Contents Properties				
Vapor Contents Absorptivity	0.1	0.1	0.1	0.1
Liquid Contents Absorptivity	0.1	0.1	0.1	0.1

Notes:

1. Two cases were run with different view factors for the Birk experiments as explained in the text.

Figure 3.1, Anderson Flame Temperature (experimental data is from Anderson et.al (1974) and model results are represented by the dashed line)
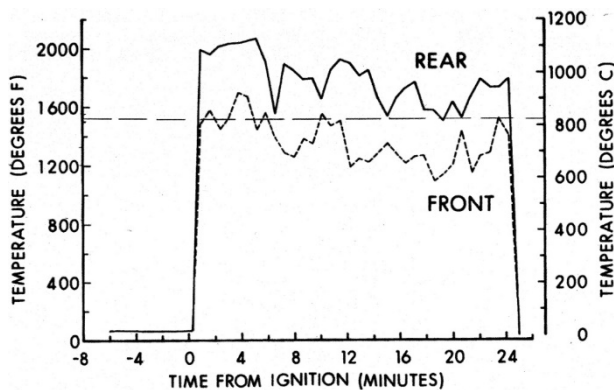
The flame emissivity was set equal to 0.94 in the Moodie case to represent a near black body, based on the dark smoke formation visible in a picture in the Moodie article. As with the Anderson case, the flame
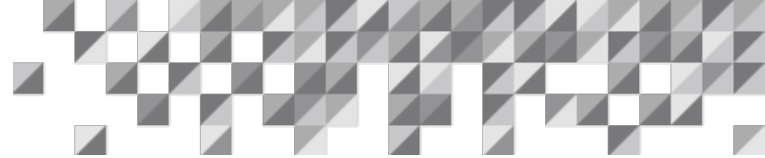
temperature was set in the Moodie case such that the calculated amount of fluid released equaled the measured value. The resulting flame temperature was 1250°F (950 K). Moodie, *et.al* (1988) reported the flame temperature to fluctuate considerably between the values of 620°F (600 K) and 1430°F (1050 K), so the model value is within the range of measured values. The measured quantities of fluid released are compared to the calculated values in Table 3.3. Agreement between measured and calculated total mass discharged was achieved with the same heat transfer parameters for all initial fill levels.

Table 3.3, Moodie Total Mass Discharged during Fire (data from Moodie et.al, 1988)

Case	22% Initial Fill	36% Initial Fill	58% Initial Fill	72% Initial Fill
Measured mass discharged, lb (kg)	1168 (530)	Not available	5018 (2276)	7496 (3400)
Calculated mass discharged, lb (kg)	1166 (529)	3397 (1541)	5080 (2304)	7173 (3254)
Difference, %	-0.2	-	1.2	-4.3

Two of the tests reported by Melhem *et.al* (1993) were modeled, Test 3 and Test 4. Both tests used liquid propane torches to simulate a pool fire and both tests started with an initial fill level of 40%. Test 3 was conducted without a PRV and the vessel burst. Test 4 was conducted with a relief device that was adequately sized. The PRV cycled twice and then failed open, safely venting the tank. Liquid inventory was constant (Test 3) or not reported (Test 4), so pressure was selected as the variable to match with the models. Propane was supplied to the torches through a series of 0.0784 inch (2 mm) diameter holes. Because of the small holes and dispersed nature of the fuel supply, it was considered appropriate to use the external convection heat transfer coefficient between the hot gases and the wall for a pool fire rather than for a jet fire as indicated in Table 3.2. Calculated pressure histories are compared to experimental data in Figure 3.2. Agreement was obtained with the same heat transfer parameters for both tests.

Figure 3.2, Melhem Pressure Profiles

Figure 3.2a, Test 3 Pressure Profile   Figure 3.2b, Test 4 Pressure Profile
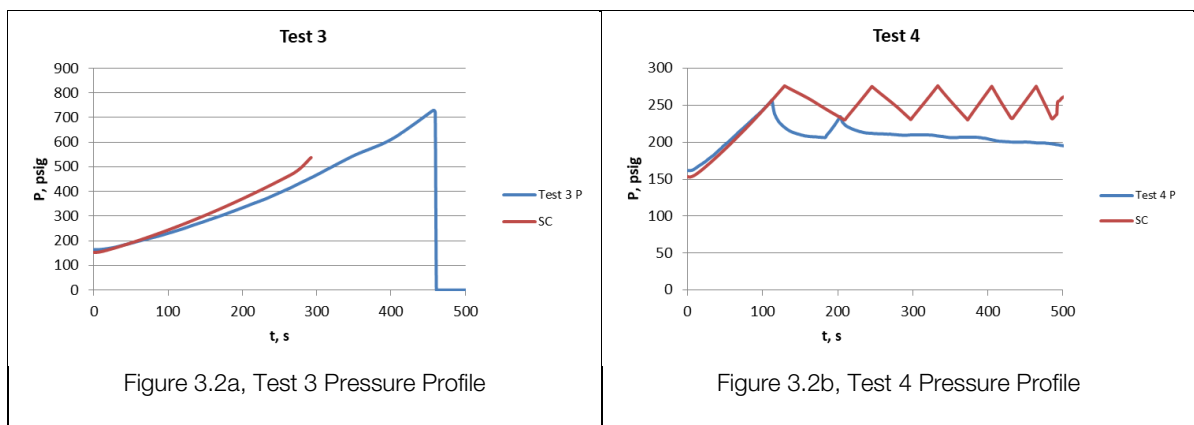
The Birk experiments were treated somewhat differently since propane torches were used rather than a pool fire in the experiments. In this case the flame emissivity and flame temperature were set to values representative of propane torches. In the first case, the geometric view factor was then set such that the
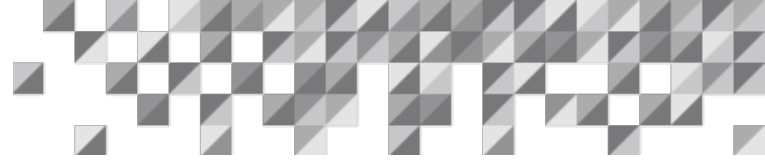
calculated amount of fluid released equaled the measured amount. Using this approach, the resulting view factor is exceedingly low and the calculated vessel wall temperature is much smaller than the measured value. The reason for this discrepancy is because of the use of torches rather than a pool fire in the experiments, and consequently a reduced amount of vessel surface heated by the flames. When the required heat input was spread over the entire vessel surface in the model, the consequence was smaller heat flux and consequently smaller calculated wall temperature.

The alternate, and recommended, approach used to model the Birk experiments was to set the geometric view factor equal to 1.0 and decrease the fraction of vessel wall exposed to the flames using vessel wall segmentation. If the top 74% of the vessel is exposed to flames in the model, then the calculated wall temperature and amount of fluid released agrees with the experimental values[1]. Birk and VenderSteen (2006) reported each of the 13 burners used in the experiments heated an area of 0.8 – 0.9 meters in diameter on the vessel surface. The calculated required heated area indicates the area heated by each torch was about 0.81 meter in diameter. The fill history comparison illustrated in Figure 3.3 indicates good model agreement with the data. The data points in Figure 3.3 represent the fill level at the time of vessel failure for various experiments.

Figure 3.3, Birk Fill History (diamond symbols indicate data from Birk et.al, 2003 and solid line is model results for 5% blowdown)
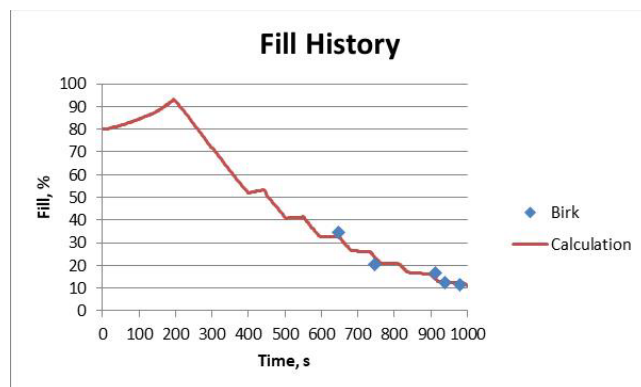
External and internal film coefficients were set to the same values for all cases, except the external convective heat transfer coefficient for the Birk case was set for a jet fire rather than a pool fire. The inside wall/liquid convective heat transfer coefficient was set to represent liquid boiling. The selected value provided internal vessel wall temperatures that approached the bulk liquid phase temperatures. Wall emissivity and absorptivity values were set based on the conditions of the vessel surfaces in the experiments. Finally, the vessel contents

---

[1] It could be argued that the vessel wall segments exposed to flames should be divided to more accurately represent the locations of the flames in the experiments. Since an equilibrium model was used, it only mattered that the correct amount of wetted vessel surface area was exposed to flames in the model.
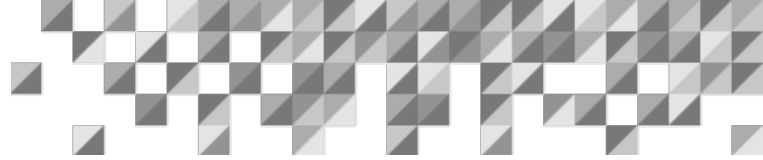
absorptivity values were specified such that the vessel inventory (essentially all propane) is nearly transparent to thermal radiation.

A modeling deficiency not often explicitly considered is the impact of jet fires on top of vessels with top mounted PRVs discharging to the atmosphere. When PRVs discharge to the atmosphere above vessels exposed to fire, the effluents often ignite and heat is radiated back to the vessels. The PRVs discharged to the atmosphere above the vessels and ignited in the Anderson, Moodie and Melhem tests. Although not explicitly considered, the heat from of the torches above the vessels was included in the calculations because the overall heat fluxes were adjusted such that the calculated rate of inventory changes (Anderson and Moodie) or rate of pressure change (Melhem) matched the data.

4. Pressure Relief Considerations

Dynamic modeling of global pressure relief scenarios, such as the fire case, in order to estimate the hydraulic performance of pressure relief effluent handling systems suggests that an important variable to know is the time to first release. Experimental results suggest the first release can occur before the liquid inventory is mixed enough to negate temperature stratification effects. Calculation results from a model that utilizes thermodynamic equilibrium are compared to experimental results in this section. The general conclusions are that equilibrium models:

1. Over-predict time to first release
2. Under-predict PRV cycling frequency

Vaporization of liquid in the thermal boundary layer in experiments, versus vaporization of bulk fluid in equilibrium-based models, accounts for both differences. Thermal stratification in experiments increases the initial pressure rise rate, thus the time to the first PRV release is less than that calculated using equilibrium models. Deviation in the time to the first release increases with initial inventory in pool fires as illustrated in Figure 4.1. In Figure 4.1, the blue diamond symbols represent comparison with data for the Anderson, Melhem and Moodie tests. For jet fires, the deviation would depend on jet location and orientation. The red square symbol represents the average of comparisons with data for the Birk tests.
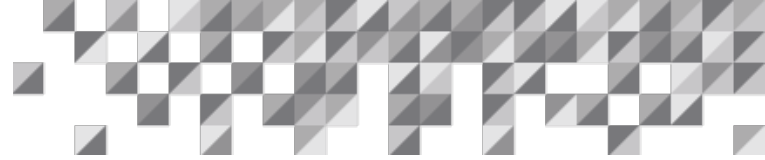
Figure 4.1, Deviation in Time to First PRV Discharge
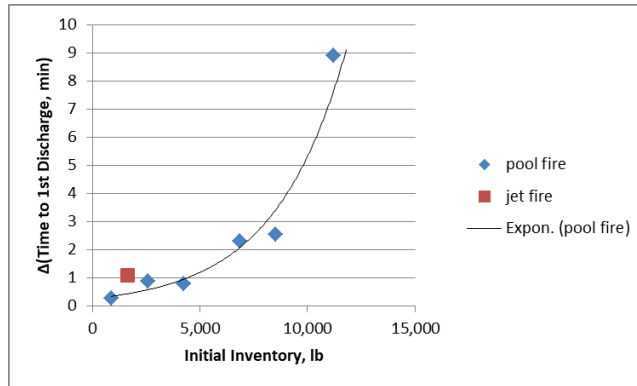
Thermal stratification and release of superheated vapor through PRVs also cause the measured pressurization/depressurization cycle times to be shorter than calculated using an equilibrium model. For small PRV blowdown values, the initial release of superheated vapor results in rapid pressure decreases with little vaporization of the bulk fluid, as seen in Figure 4.2a. For larger PRV blowdown values, the initial release of superheated vapors is followed by vaporization from the bulk fluid, as illustrated in Figures 4.2c and 4.2e. The change in slope after the rapid pressure decrease is indicative of bulk fluid vaporization commencing. On the other hand, vapor-liquid equilibrium in equilibrium models indicates that vapor releases are concomitant with bulk liquid vaporization. The rapid pressure decreases in the experiments, due to vapor superheating, allows the PRVs to more quickly reseat at the blowdown pressures than is calculated using equilibrium models, as seen by comparing the graphs of the experiments on the left to graphs of the model results on the right in Figure 4.2. Deviation in PRV cycle time also depends on PRV blowdown as can be seen by comparing experimental results to calculation results in Figure 4.2. The effects of rapid PRV cycle time on valve stability are unknown. Generally, re-pressurization caused by fire exposure after a PRV reseats takes a longer time than a typical PRV opening/closing time. This leads at best to low frequency cycling which is considered a stable behavior.

Given the pressurization/depressurization dynamics, the calculated pressures as a function of time are unlikely to match the measured values; at least until temperature homogeneity is achieved in the experiments. The good news is that the calculated peak pressure equals the measured peak pressure when the model parameters are set such that the calculated amount of fluid released during the fire matches the measured value. See Figure 4.3, from Anderson, as an illustration of measured versus calculated pressure profiles. The peak measured pressure was obtained in the Anderson experiment after temperature de-stratification of the liquid phase was complete.
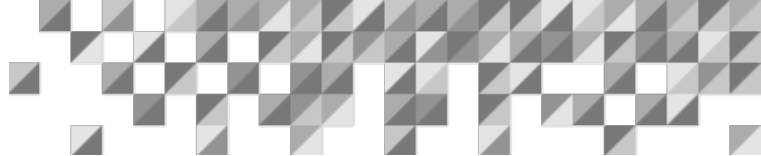
Figure 4.2, Birk PRV Cycle Time Comparison (experimental data on the left from Birk *et.al,* 2003[2] and model results on the right)

Figure 4.2a, 5% Blowdown Experiment

Figure 4.2b, 5% Blowdown Model

Figure 4.2c, 30% Blowdown Experiment

Figure 4.2d, 30% Blowdown Model

Figure 4.2e, 45% Blowdown Experiment

Figure 4.2f, 45% Blowdown Model

---
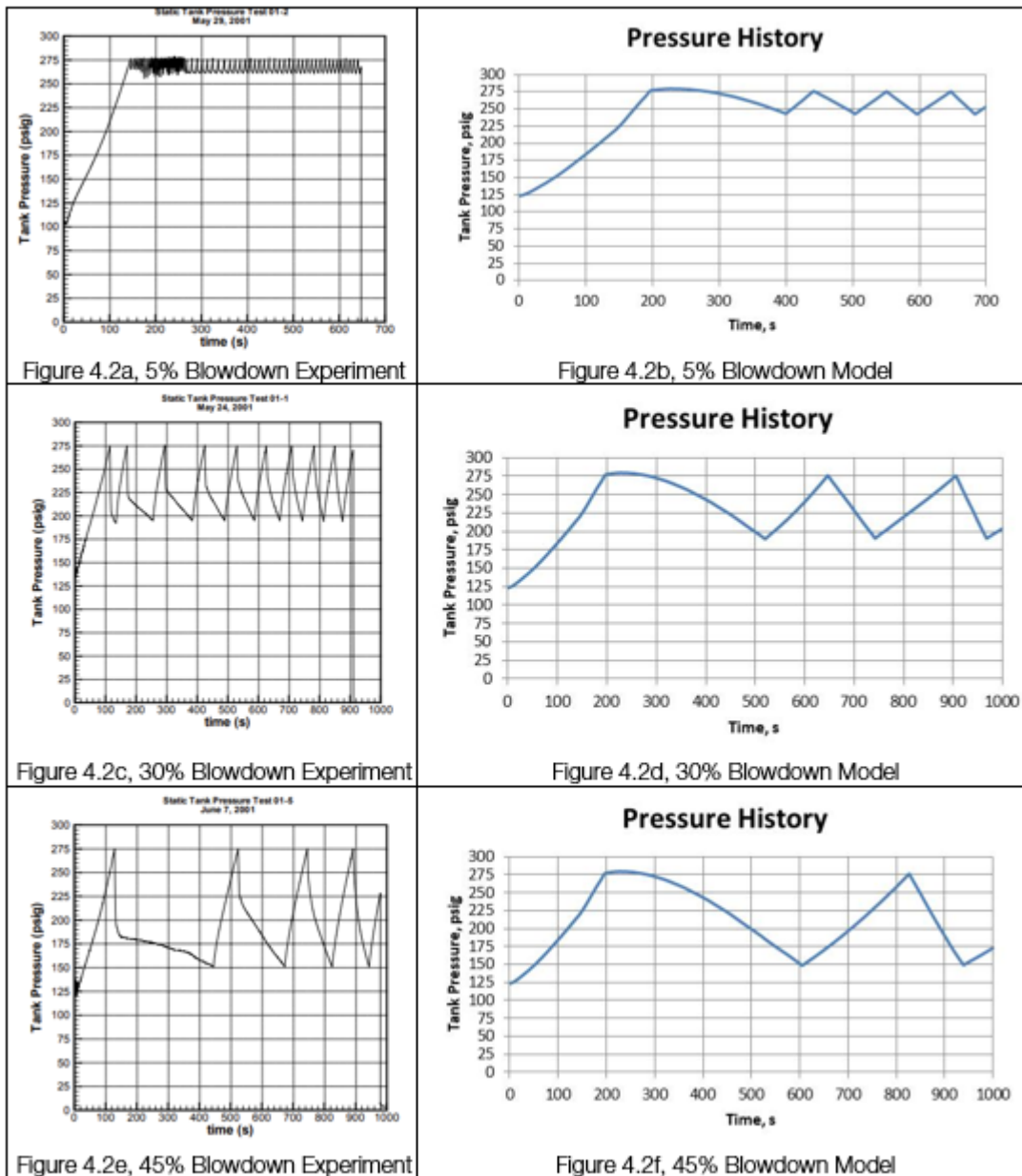
[2] Note definition of blowdown by Birk, *et.al* was different from that in SuperChems^{TM}. Birk *et.al* defined blowdown as $(P_{open}\text{-}P_{close})/P_{open}$ whereas in SuperChems^{TM} blowdown is defined as $(P_{set}\text{-}P_{close})/P_{set}$. Consequently, for the 5% blowdown case in Birk *et.al*, the closing pressure is higher than the set pressure, which is not allowed in SuperChems^{TM}. Thus for this case, the closing pressure was arbitrarily lowered to 245 psig in the model, which results in 2% blowdown using the SuperChems^{TM} definition. For the 30% and 45% blowdown cases in Birk et.al, the same closing pressure was used in the model, rather than the same value of blowdown.
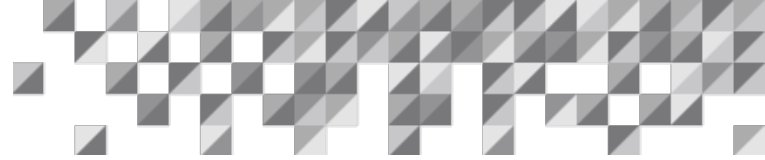
Figure 4.3, Anderson Pressure Profiles (continuous curve is data from Anderson *et.al* (1974) and calculated pressure values are indicated by + signs)
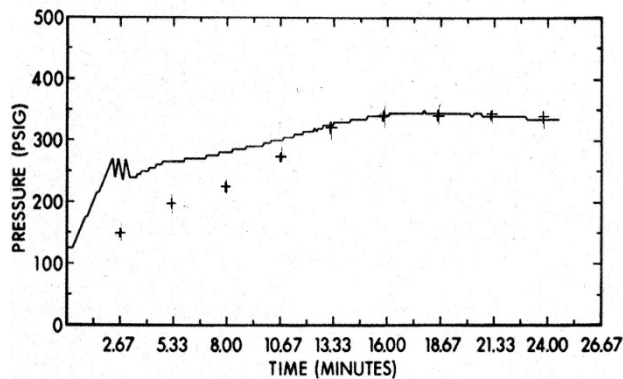
5. Wall Temperature and Vessel Rupture Considerations

In order to estimate the potential for wall rupture, it is important for the coincident wall temperature and vessel pressure to be estimated relatively accurately. If the estimated rate of increase of either wall temperature or vessel pressure lags the actual rate of increase, then the potential exists for incorrectly estimating the time for the potential vessel rupture. In the cases discussed below, the model parameters were set such that the calculated quantities of fluid released equaled the measured quantities released (Anderson, Birk and Moodie) or the pressure profile was matched directly (Melhem). Consequently, the calculated peak pressures also matched the measured values.

A result of modeling the Anderson experiment is illustrated in Figure 5.1. The calculated vapor wall temperature initially increases faster than the measured value, but the calculated final wall temperature agrees with the measured value. The model indicated a potential for vessel rupture occurs at about 17 minutes (0.283 hr). The actual vessel rupture occurred at 24.5 minutes (0.408 hr). At 17 minutes, the calculated and measured vapor wall temperatures were essentially equal, so temperature difference does not account for the deviation in estimated time to failure. Also note that the estimated time to failure can be increased by using the ultimate stress rather than the ASME allowed stress. It is likely that using the ultimate stress in this case could improve the estimated time to failure, but using the allowed stress compensates for any potential defects in materials and workmanship so in general is still recommended.

A result of modeling the Moodie experiments is illustrated in Figure 5.2. The calculated vapor wall temperature matches the measured vapor wall temperature fairly well for the 72% fill level, but it deviates from measured values for lower fill levels (Table 5.1). The amount of deviation increases as the initial fill level decreases. A possible explanation of this phenomenon was initially thought to be that the equilibrium model failed to capture the vapor wall heat-up rate at low initial fill levels because it failed to account for vapor superheating. It turns out that in vapor inside heat transfer coefficient (convection plus radiation) is small enough that the vapor wall
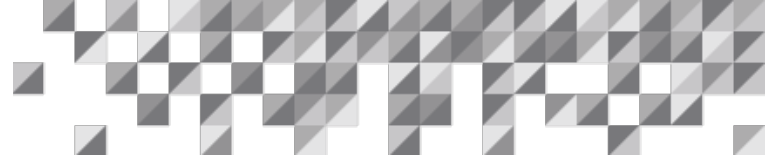
temperature increase rate is insensitive to the inside vapor temperature, as illustrated in Figure 5.3. In Figure 5.3, the wall temperature history is illustrated for two different vapor temperatures, 125°F (326 K) and 575°F (575 K). It can be seen that the rate of wall temperature increase is essentially the same for both vapor temperatures. Obviously increasing the heat flux to the wall would increase the wall temperature heat-up rate for lower initial fill levels. Unfortunately, increasing the heat flux would also result in releasing too much fluid through the PRV. The wall failure stress history indicated wall failure was unlikely for all initial fill levels, which matches the experiments since the vessel did not actually fail (Figure 5.2b). Determination of why the calculated vapor wall temperatures appear to deviate from the measured values for lower initial fill levels is recommended.

Figure 5.1, Anderson Wall Temperature and Wall Stress Histories (data from Anderson *et.al* (1974) and calculated wall temperature values are indicated by + symbols)

| Figure 5.1a, Wall Temperature | Figure 5.1b, Wall Failure Stress History |
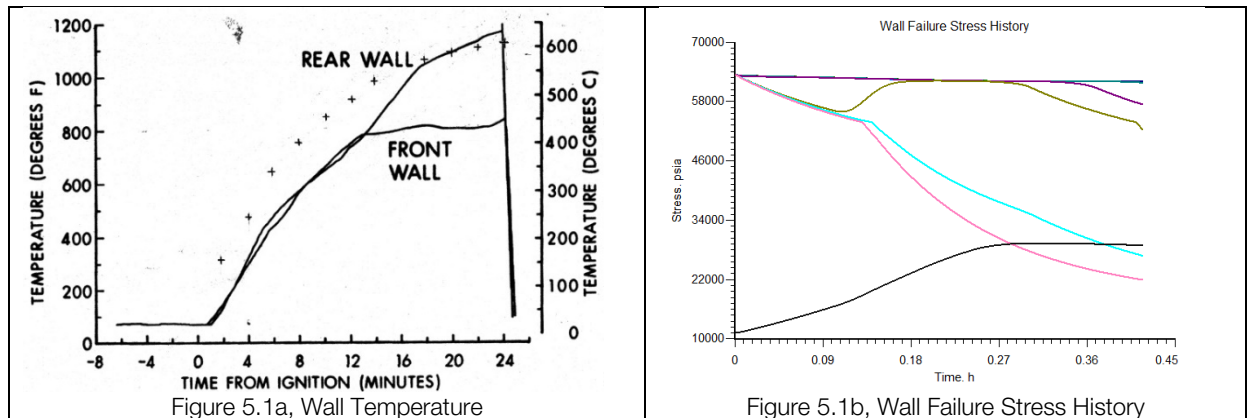
Figure 5.2, Moodie Wall Temperature and Wall Stress Histories (data from Moodie, *et.al* (1988) and calculated wall temperature values are indicated by + symbols)

Figure 5.2a, Wall Temperature

Figure 5.2b, Wall Failure Stress History (72% initial fill level)
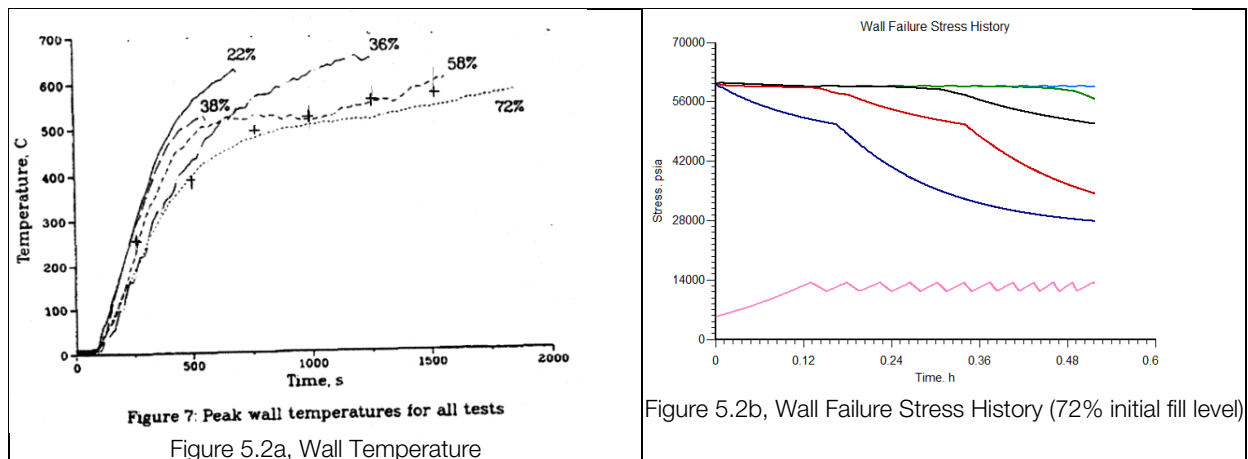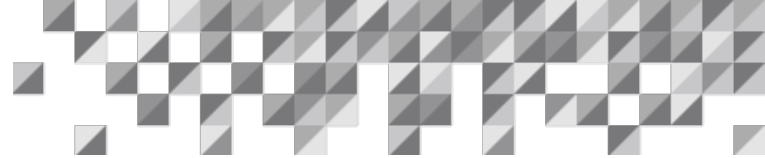
Table 5.1, Moodie Maximum Skin Temperature (data from Moodie *et.al*, 1988)

Case	22% Initial Fill	36% Initial Fill	58% Initial Fill	72% Initial Fill
Measured maximum skin temperature, °F (K)	1175 (908)	1215 (930)	1130 (883)	1062 (845)
Calculated maximum skin temperature, °F (K)	836 (720)	1007 (815)	1039 (833)	1097 (865)
Difference, %	-28.9	-17.1	-8.1	3.3

Figure 5.3, Calculated Vapor Wall Temperature History for Two Different Vapor Temperatures
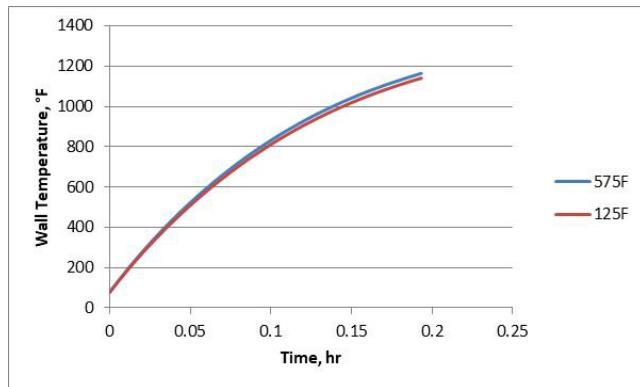
Birk used propane torches rather than a pool fire in his experiments. Because the vessel was not totally engulfed in flames, this difference in experimental procedure made the modeling more like the vessel was exposed to a jet fire rather than a pool fire. The vapor wall temperature profiles are illustrated in Figure 5.4a. In Case 1, the calculated heat flux was spread over the entirety of the vessel. In this case, the calculated quantities of fluid released matched the measured quantities for the five experiments modeled. Unfortunately, the calculated vapor wall temperatures were extremely low, as indicated by the + symbols. The resulting wall failure stress history indicated the vessels should not have failed for this case (Figure 5.4b), even though all five of the vessels did fail in the experiments. This case illustrates the dangers of modeling jet fires as if they were pool fires.

In case 2, the majority of the heat flux was directed to the portion of the vessel walls initially exposed to the vapor phase. In this case the calculated vapor wall temperatures more closely match the measured values as indicated by the o symbols in Figure 5.4a. The wall failure stress history illustrated in Figure 5.4c indicates the potential for wall failure occurs at about 5.6 minutes (0.093 hr). Actual times to failure were longer than the estimated time as indicated in Table 5.2. Once again, it would be possible to extend the estimated time to failure by using the ultimate stress values rather than the ASME allowable values. However, Birk *et.al* performed a failure analysis and concluded that for the type of heating employed the assumption that failure occurs when the hoop stress exceeds the material ultimate strength was not justified because of the small heated length. They improved the predicted time to failure by using 1.5 times the ultimate strength and also
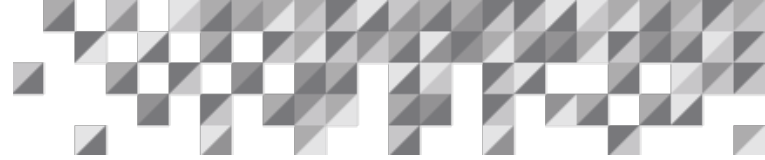
proposed that it may be more reliable to use Von Mises stress rather than hoop stress when the heat source localized as opposed to totally engulfed, as in a pool fire.

Figure 5.4, Birk Wall Temperature and Wall Stress Histories (data from Birk *et.al* (2003) and calculated wall temperature values are indicated by + symbols for case 1 and by o symbols for case 2)
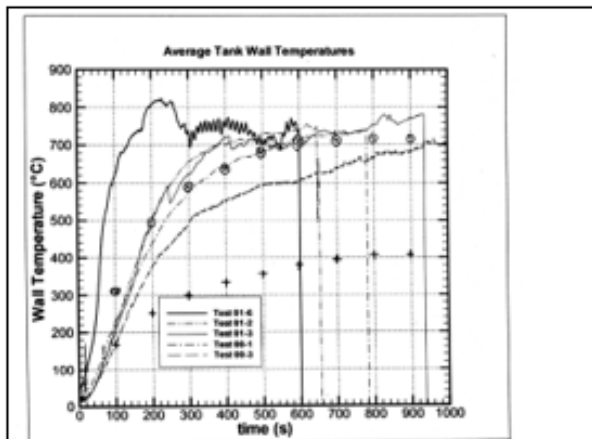
Figure 5.4a, Wall Temperature
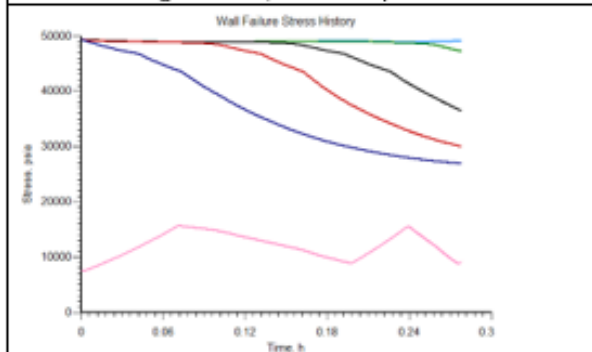
Figure 5.4b, Case 1 Wall Failure Stress History
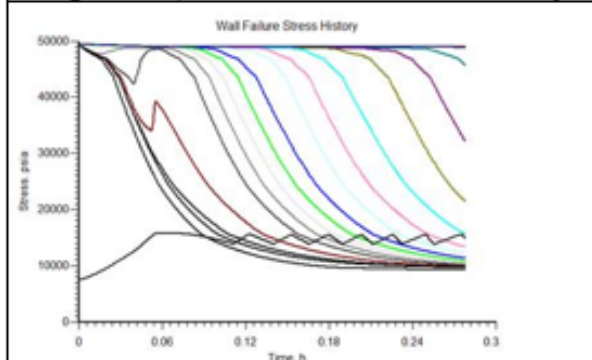
Figure 5.4c, Case 2 Wall Failure Stress History
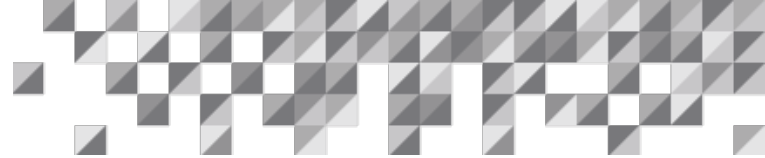
Table 5.2, Birk Experimental Time to Failure (data from Birk *et.al*, 2003)

Blowdown, %	Time to Failure, min
5	10.8-12.4
30	15.2-15.6
45	16.3

Melhem test data is compared to SuperChems™ modeling results in Figure 5.5. In these tests, four thermocouples were attached to the external wall of the test vessels above the vessel centerline and four were attached below the vessel centerline. The data from the top four thermocouples were averaged and labeled "top TI data" in Figure 5. Likewise, data from the bottom four thermocouples were averaged and labeled "bottom TI data" in Figure 5. Data from the temperature indicators are compared to model results in Figures 5.5a and 5.5c. Curves labeled "top SC" and "bottom SC" are the SuperChems™ model results for the top and bottom vessel segments, respectively. The model results for both cases are similar, as would be expected since the same vessels were modeled with the same fire parameters. The data indicates the wall temperatures were hotter in Test 3 than Test 4, for unknown reasons. The wall temperature data in Test 4 are more variable than in Test 3, likely in response to the PRV discharging. Model results show reasonable agreement with Test 4 temperature data.

Calculated wall failure stress histories are shown in Figures 5.5b and 5.5c for Test 3 and Test 4, respectively. The model of Test 3 predicts a potential for failure at around 0.079 hr (284 s) while actual failure occurred at 0.127 hr (458 s). The model of Test 4 predicts a potential for failure at around 0.167 hr (601 s) while actual failure did not occur. The Melhem tests times to failure are summarized in Table 5.3. Once again, the estimated times to failure are conservative.

Figure 5.5, Melhem Wall Temperature and Wall Failure Stress Histories

Figure 5.5a, Test 3 Wall Temperatures   Figure 5.5b, Test 3 Wall Failure Stress History
Figure 5.5c, Test 4 Wall Temperatures   Figure 5.5d, Test 4 Wall Failure Stress History
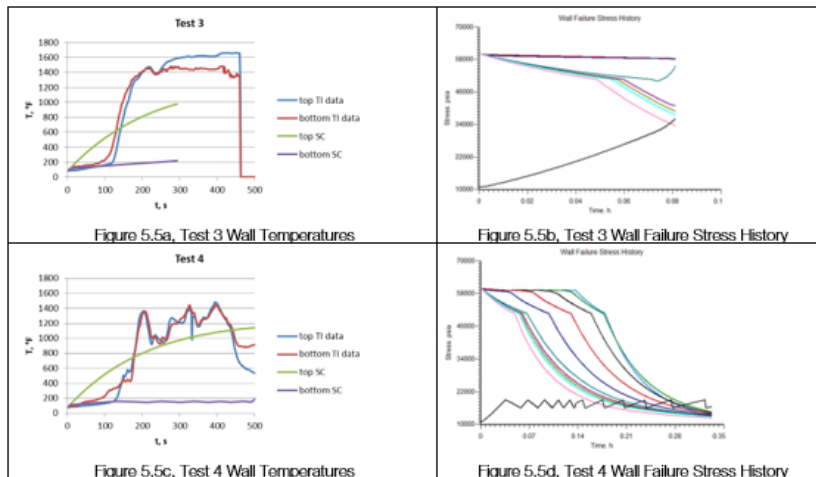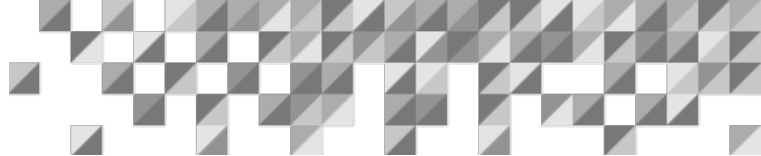
Table 5.3 Melhem Times to Failure

Test	Actual Failure Time, s	Estimated Failure Time, s
3	458	284
4	No failure	601

6. Comparison with API Standard 521 Recommended Flux Values

API Standard 521 provides recommended values for heat transfer parameters to use when other data or information are not available. The standard further recommends using one set of parameters for sizing pressure relief devices designated as the surface average heat flux and a second set of parameters for estimating the time to failure designated as local peak heat flux. The API recommended values for surface average heat flux are summarized in Table 6.1 and for local peak heat flux in Table 6.2. In Tables 6.1 and 6.2, the fire heat flux was calculated by neglecting the convective heat transfer and setting the tank temperature equal to zero

$$q_{fire} = \epsilon_{fire} \sigma T_{flame}^4$$

Note this fire heat flux is not the same as that reported in API Standard 521 in which the convective heat flux was included and calculated assuming the surface temperature is 122°F (323K).

The amount of heat absorbed by the vessel was then calculated by including the surface absorptivity and geometric view factor

$$q_{in} = \propto_{surface} F_{12} q_{fire}$$

The API Average absorbed heat flux is 77.03 Btu/in^2 hr (34.96 kW/m^2). The Anderson absorbed heat flux was 103.26 Btu/in^2 hr (46.86 kW/m^2) and the Melhem absorbed heat flux was 105.93 Btu/in^2 hr (48.07 kW/m^2), so the API average heat flux is less than measured in these cases. The Moodie absorbed heat flux was 76.71 Btu/in^2 hr (34.81 kW/m^2) and the Birk absorbed heat flux was 78.16 Btu/in^2 hr (35.47 kW/m^2), so the API Average heat flux is about right in these cases. The API average heat flux parameters were used directly as a comparison with base case parameters. These cases illustrate a potential offset in the Anderson and Melhem cases.

When estimating the time to failure it is important that the calculated wall temperature and corresponding pressure are coincident in time. Unfortunately, for fixed pressure relief device capacity, if the API peak heat flux parameters were applied to the entire vessel surface area then the calculated pressure would increase too rapidly. The result would be that the estimated time to failure would be too conservative. In order to maintain the proper rate of pressure increase, it is recommended to decrease the amount of surface area exposed to fire in the model.
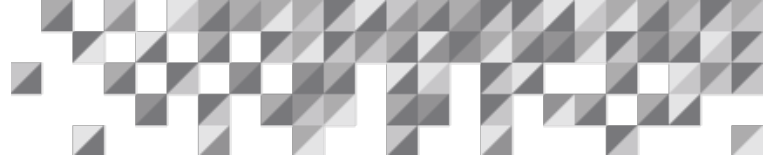
The API Peak absorbed heat flux for pool fires is 215.42 Btu/in^2 hr (97.76 kW/m^2), which is larger than the Anderson, Melhem and Moodie cases. The API Peak absorbed heat flux for small jet fires is 249.87 Btu/in^2 hr (113.40 kW/m^2), which is larger than any of the three test cases. In order to estimate the wall temperature history concurrent with the vessel pressure history, the vessel external surface area exposed to fire was reduced as summarized in Table 6.2. In the Anderson case the wall segments exposed to fire would represent 48% of the external surface area. In the Moodie, Melhem and Birk cases the wall segments exposed to fire would represent about 36%, 49% and 31% of the external surface area, respectively.

In SuperChems^{TM}, the user is able to divide the vessel wall into numerous segments and then specify which of those segments are exposed to the fire. At least one of the wall segments in contact with the vapor phase inventory should be exposed to the fire in order to estimate the peak wall temperature. The number of wall segments in contact with the liquid phase inventory, i.e., the wetted area, should be reduced such that the desired wetted area is obtained. In practice, the vessel top segment was retained and then segments under the top one were sequentially removed until the desired surface area was obtained. Results are illustrated in Figures 6.1 through 6.4.

In the Anderson case (Figure 6.1), the API Average flux case provided a smaller rate of pressure and temperature increase. Conversely, the API Peak flux case provided a pressure increase rate that matched the base case pressure increase but the peak wall temperature was considerably larger than the other cases. In this case the API Average case heat flux parameters indicated the vessel wall was unlikely to fail, i.e., a false negative. The API Standard 521 warns that it is not appropriate to use the surface average heat flux to estimate if the vessel wall is likely to fail. Conversely, the estimated time to failure using the API Peak heat flux parameters was smaller than both the Base case and the actual failure time.

In the Moodie case (Figure 6.2) the rate of pressure rise and the peak pressure was similar for all three cases. Once again, the predicted peak vessel wall temperature when using the API Peak heat flux case parameters was considerable larger than the other cases. The API Peak heat flux case also predicted the vessel would fail when it actually did not fail, i.e., a false positive. The API Peak heat flux parameters likely are conservative for pool fires of liquid hydrocarbons such as gasoline, kerosene or diesel.

In the Birk case (Figure 6.3), the predicted pressure history was similar for all three cases and the API Peak heat flux parameters provided a peak wall temperature considerably larger than the other two cases. The increased wall temperature in the API Peak heat flux case resulted in decreased estimated time to failure. The calculated time to failure was less than the measured values for all three cases. The API Peak heat flux parameters are also likely conservative for propane jet fires.

In the Melhem case (Figure 6.4), the API Average flux case provided a smaller rate of pressure and temperature increase. Conversely, the API Peak flux case provided a pressure increase rate that matched the base case pressure increase but the peak wall temperature was considerably larger than the other cases. In this case
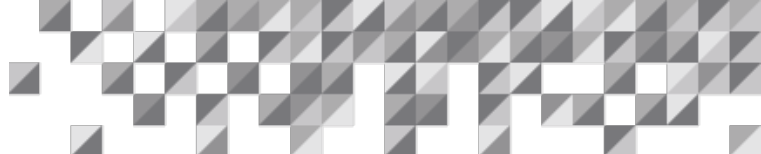
the API Average case heat flux parameters indicated the vessel wall was unlikely to fail during the duration of the fire, i.e., a false negative. The API Standard 521 warns that it is not appropriate to use the surface average heat flux to estimate if the vessel wall is likely to fail. Conversely, the estimated time to failure using the API Peak heat flux parameters was smaller than both the Base case and the actual failure time.

Table 6.1, Methodology for API Surface Average Heat Flux Cases

Case	API Pool Fire Average	Anderson Base Case	Moodie Base Case	Melhem Base Case	Birk Base Case	Birk API Jet Fire Average
ε_{fire}	0.75	0.62	0.94	0.33	0.33	0.33
σ, Btu/ft^2 hr °R^4 (W/m^2 K^4)	1.7130E-09 (5.6704E-08)	1.7130E-09 (5.6704E-08)	1.7130E-09 (5.6704E-08)	1.7130E-09 (5.6704E-08)	1.7130E-09 (5.6704E-08)	1.7130E-09 (5.6704E-08)
T_{gas}, °F (K)	1112 (873)	1526 (1103)	1251 (950)	1880 (1300)	1880 (1300)	1652 (1173)
T_{flame}, °F (K)	1382 (1023)	1526 (1103)	1251 (950)	1880 (1300)	1880 (1300)	2012 (1373)
q_{fire}, Btu/ft^2 hr (kW/m^2)	14,790 (46.60)	16,522 (52.06)	13,808 (43.51)	16,949 (53.41)	16,949 (53.41)	21,109 (66.53)
q_{fire}, Btu/in^2 hr (kW/m2)	102.71 (46.60)	114.73 (52.06)	95.89 (43.51)	117.70 (53.41)	117.70 (53.41)	146.59 (66.53)
$\alpha_{surface}$	0.75	0.90	0.80	0.90	0.90	0.75
F_{12}	1	1	1	1	1	1
q_{in}, Btu/in^2 hr (kW/m^2)	77.03 (34.95)	103.26 (46.86)	76.71 (34.81)	105.93 (48.07)	105.93 (48.07)	109.94 (49.90)
A_{fire}/A_{vessel}	1	1	1	1	0.7378	0.7382
Adjusted Q_{in}, Btu/in^2 hr (kW/m^2)	77.03 (34.95)	103.26 (46.86)	76.71 (34.81)	105.93 (48.07)	78.16 (35.47)	81.12 (36.81)

Table 6.2, Methodology for API Peak Heat Flux Cases

Case	API Pool Fire Peak	Anderson API Peak	Moodie API Peak	Melhem API Peak	Birk API Small Jet Fire Peak
ε_{fire}	0.75	0.75	0.75	0.75	0.75
σ, Btu/ft^2 hr °R^4 (W/m^2 K^4)	1.7130E-09 (5.6704E-08)	1.7130E-09 (5.6704E-08)	1.7130E-09 (5.6704E-08)	1.7130E-09 (5.6704E-08)	1.7130E-09 (5.6704E-08)
T_{gas}, °F (K)	1922 (1323)	1922 (1323)	1922 (1323)	1922 (1323)	2012 (1373)
T_{flame}, °F (K)	1922 (1323)	1922 (1323)	1922 (1323)	1922 (1323)	2012 (1373)
q_{fire}, Btu/ft^2 hr (kW/m^2)	41,360 (130.35)	41,360 (130.35)	41,360 (130.35)	41,360 (130.35)	47,975 (151.20)
q_{fire}, Btu/in^2 hr (kW/m2)	287.23 (130.35)	287.23 (130.35)	287.23 (130.35)	287.23 (130.35)	333.16 (151.20)
$\alpha_{surface}$	0.75	0.75	0.75	0.75	0.75
F_{12}	1	1	1	1	1
q_{in}, Btu/in^2 hr (kW/m^2)	215.42 (97.76)	215.42 (97.76)	215.42 (97.76)	215.42 (97.76)	249.87 (113.40)
A_{fire}/A_{vessel}		0.4793	0.3561	0.4918	0.3128
Adjusted Q_{in}, Btu/in^2 hr (kW/m^2)		103.26 (46.86)	76.71 (34.81)	105.93 (48.07)	78.16 (35.47)
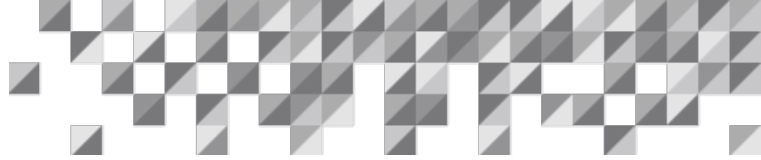
Figure 6.1, Anderson Results Comparison

Case	Time to failure, min
Actual	24.5
Calculated	
Base	17
API Average	NA
API Peak	8.2
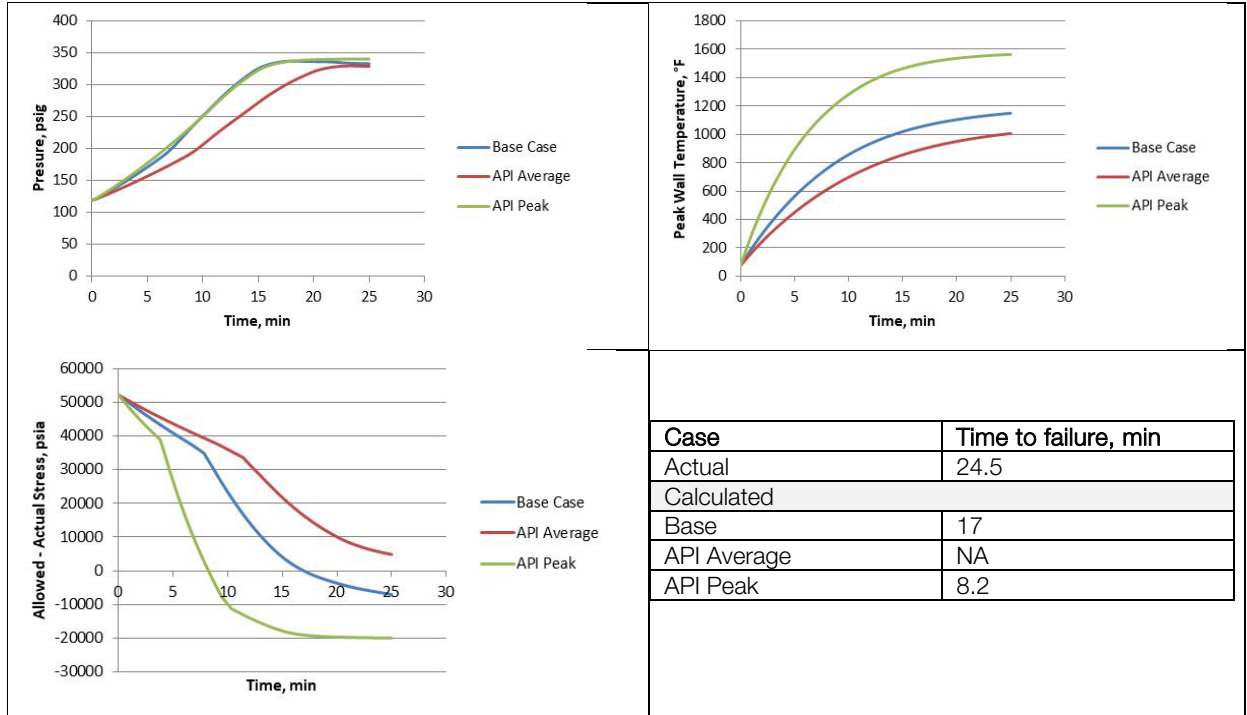
Figure 6.2, Moodie 72% Fill Results Comparison

Case	Time to Failure, min
Actual	NA
Calculated	
Base	NA
API Average	NA
API Peak	7.1
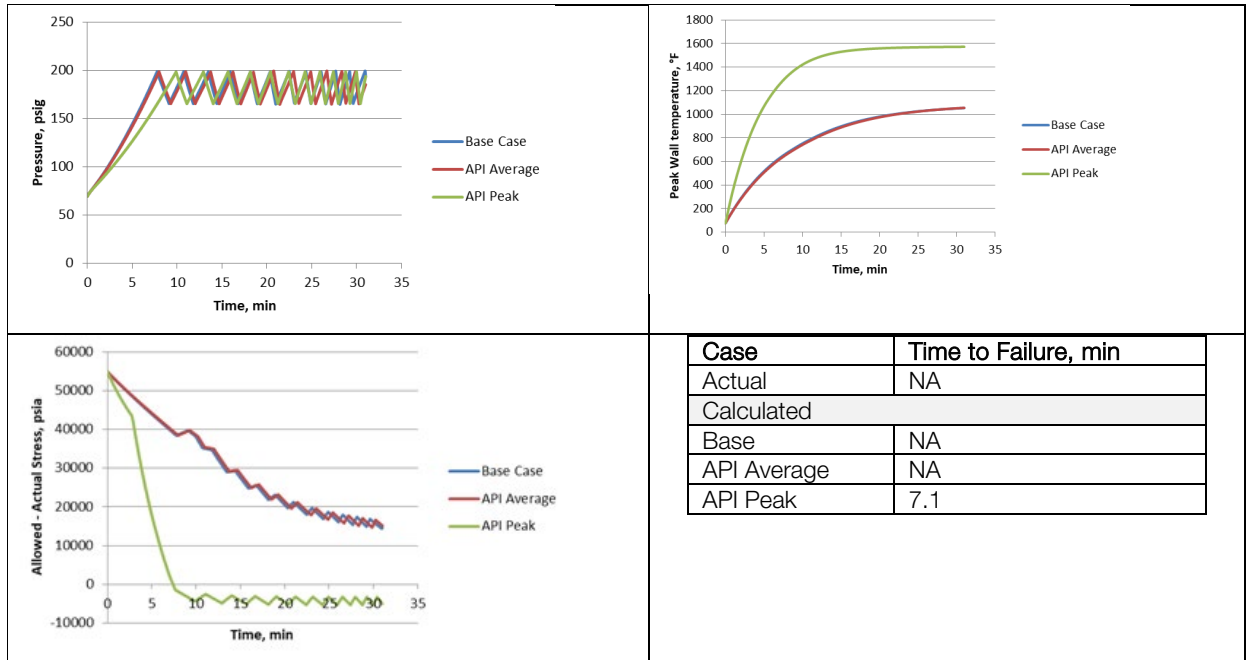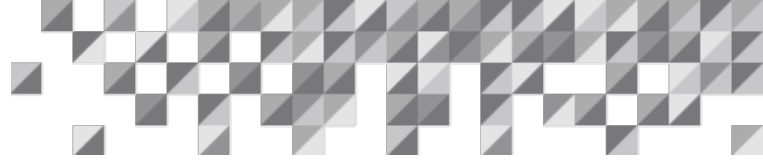
Figure 6.3, Birk 5% Blowdown Results Comparison

Case	Time to failure, min
Actual	
5% blowdown	10.8, 12.4
30% blowdown	15.2, 15.5
45% blowdown	16.3
Calculated (5% blowdown)	
Base	5.6
API Average	6.1
API Peak	3.0
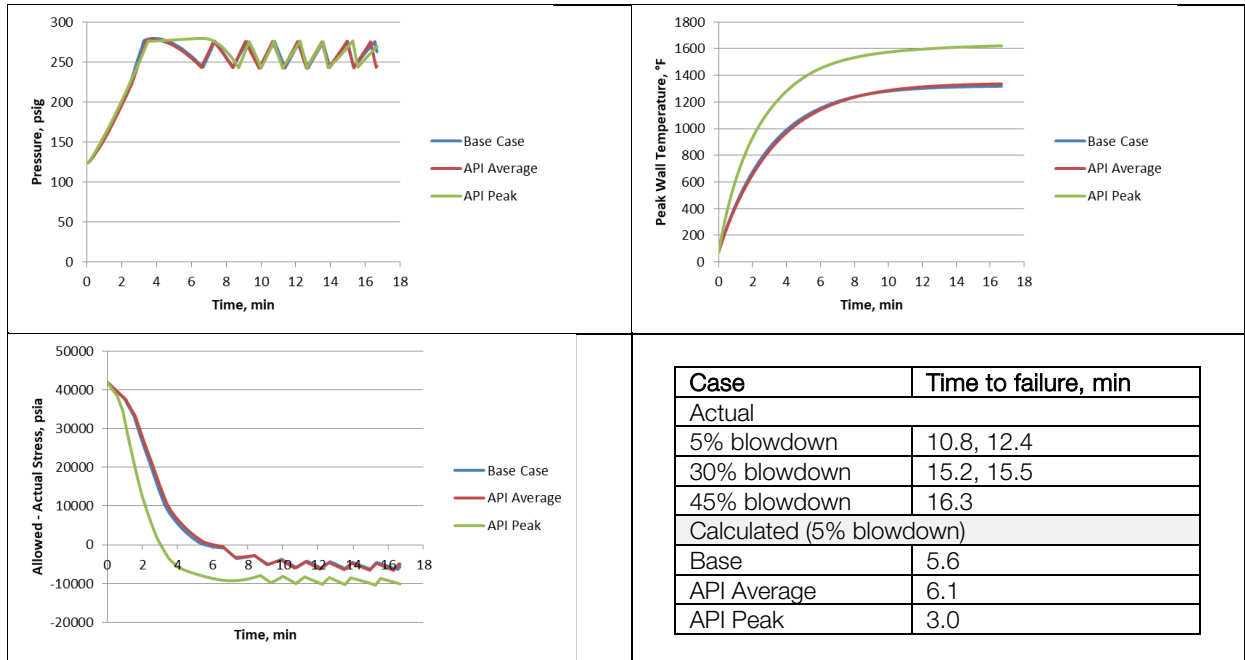
Figure 6.4, Melhem Test 3 Results Comparison

Case	Time to Failure, min
Actual	7.6
Calculated (Test 3)	
Base	4.7
API Average	NA
API Peak	2.9
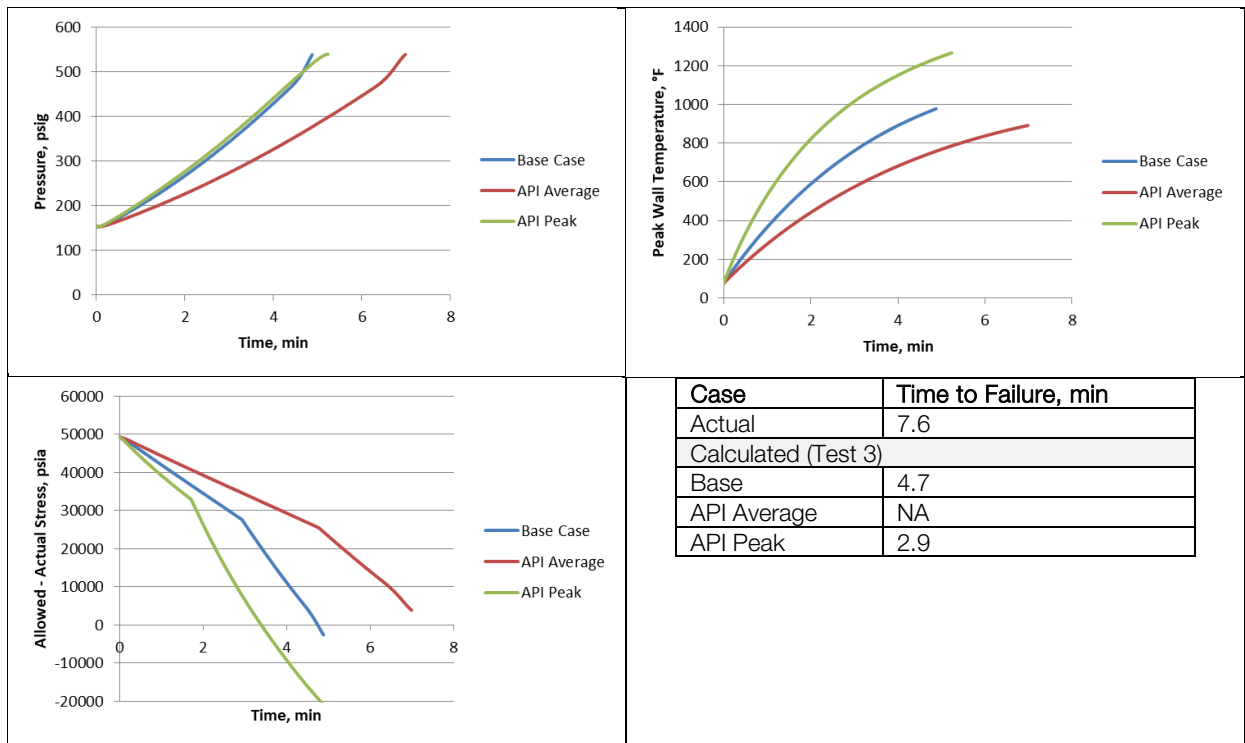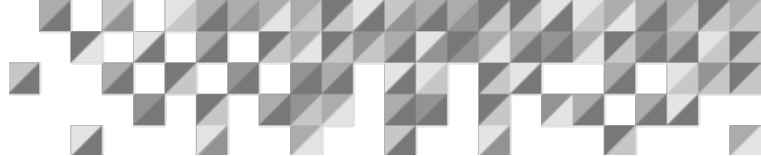
7. Vessels Containing Reactive Chemicals Exposed to External Fire

Chemical reactions can significantly change the required relief rates. Since most chemical reactions have exponential temperature dependence, the reaction heat can quickly dwarf fire heat effects (DIERS, 2017). To the authors knowledge, no large-scale tests have been reported that have demonstrated non-equilibrium effects under external fire exposure, e.g., liquid thermal stratification and vapor superheating.

Because chemical reactions (vapor/tempered, gassy, or hybrid) generate vapor and/or non-condensable gases in bulk, vessel contents are expected to exhibit substantial mixing. As a result, the assumption of equilibrium between the vapor and liquid phases is valid as demonstrated by current best practices for developing relief requirements for runaway reactions (see Melhem, 2021).

It is also important to note that runaway reactions can often lead to multiphase flow. When multiphase flow occurs, the heat stored in the vessel vapor walls due to fire exposure is recovered by the multiphase mixture as it coats the vapor walls.

8. LNG Pool Fires

The case of LNG pool fires deserves special consideration. LNG pool fires are luminous until the LNG light ends are completely fractionated by fire. LNG flames emissive powers have been reported in excess of 200 kW/m2 and as high as 300 kW/m2 (see Melhem 2009 and 2011) even for large pool fires (see Sandia publication on 100 m pool experiments). For LNG pool fires, the flame temperatures used for modeling of fire exposure will be higher than what is recommended by API 521 for typical pool fires.

9. Conclusions

We have demonstrated in this paper that the equilibrium models in SuperChems™ can reproduce important aspects of large-scale fire exposure experiments and measurements. Using the guidance provided in this paper, SuperChems™ can be used to develop realistic estimates of relief requirements and estimated time to fail or yield.

Dynamic modeling of pressure relief systems, including PRV dynamics and effluent handling systems, can be used to both validate the adequacy of those systems and also design new systems, e.g., API Standard 521. Various scenarios can be modeled for common mode events, such as fire exposure, using state of the art dynamic models.

Models based on thermodynamic equilibrium do not capture all effects encountered during fire exposure, such as thermal stratification and subsequent mixing. Since mixing is most prevalent while the PRV is open and peak relief flow rates do not occur until after the liquid phase is well mixed, calculations that depend on the estimated time to first release, such as hydraulic performance of headers found in pressure relief systems,
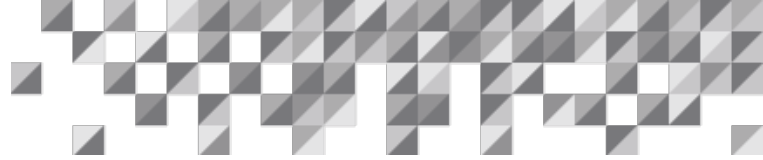
should be used with caution because it is likely that flow will occur before it is estimated to happen. Since peak relief flow rates occur after the liquid mixing is complete, a cautious approach to estimating effluent handling systems hydraulics is to use pressure relief valve flow rates that occur after the thermal stratification and mixing times have elapsed.

Estimating the time to failure of pressure vessels exposed to fires depends on accurately predicting the coincident temperatures and pressures. This estimated time is also the most reliable after the thermal stratification and mixing times have elapsed and the thermodynamic equilibrium assumption is valid. Good estimates of the flame temperatures and emissivity values are essential to predict the vessel wall temperature history. A quality database summarizing these values would be welcomed. The radiation absorptivity of the vessel contents greatly impacts the estimated vessel wall temperature, especially for the vessel wall in contact with vapors. It is possible to estimate the absorptivity values from infrared spectra, but again, a good database of recommended values would be welcomed. Tables containing emissivity values of various surfaces exist, so these values are more readily available.

For vessels totally engulfed in flames from pool fires the surface average heat flux can be used to estimate both the quantity of fluid released and the vessel wall temperatures during an event. Selection of the proper metal stress values should then result in reasonable estimates of the time to failure. When a pool fire is simulated with torches or when a vessel is exposed to a jet fire, using the local peak heat flux is necessary to estimate the wall temperature history, but the quantity of fluid relieved is over-predicted unless the heat flux is limited to the vessel surface area exposed to the flames. The proper stress values to use with jet fires has also been questioned since the hoop stress over the entire wall does not necessarily reflect the allowable stress on the portion of the vessel wall that is overheated.

API Standard 521 recommends using the pool fire surface average heat flux parameters for sizing pressure relief valves. The Standard provides ranges for the values of parameters to use when modeling pool fires as well as recommended values "where other data or information are unavailable". Modeling with values recommended "where other data or information are unavailable" should be done with caution. Calculated heat fluxes that result from using those values may be lower than actually experienced, as for example in the Anderson test. Engineering judgement when selecting modeling parameters is recommended, especially when selecting the fire temperature.

API Standard 521 also recommends using local peak heat fluxes when estimating time to failure of the vessel walls. Applying the local peak heat flux parameters to the fire exposed vessel surface area results in overestimating the pressurization rate and the peak pressure. The result is overly conservative estimates of the possible time for vessel failure. Reducing the surface area exposed to the peak heat flux can be used to alleviate over conservative estimates of the vessel pressure and thus provide improved estimates of the time to failure.
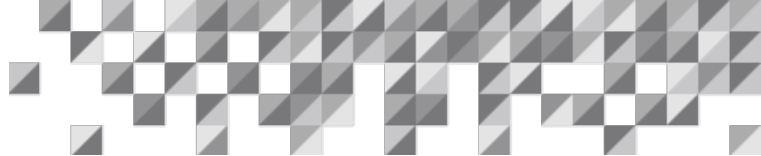
10. Acknowledgements
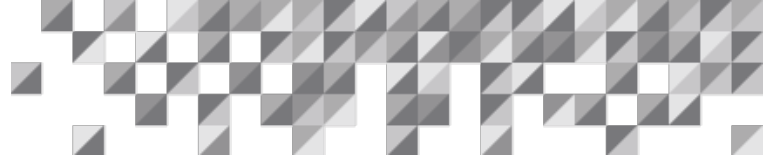
Authors

Greg Hendrickson; greghendrickson1954@gmail.com

Georges A. Melhem; melhem@ioMosaic.com
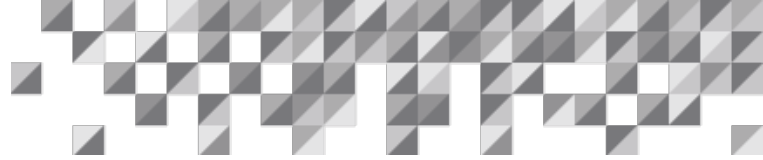
Nomenclature

A   heat transfer area (ft^2, m^2)

F_{12} geometric view factor

h   convective heat transfer coefficient (Btu/ft^2 hr °F, W/m^2 K)

Q   heat transfer rate, Btu/hr (W)

q   heat flux, Btu/ft^2 hr (W/m^2)

T_{flame} flame temperature (°R, K)

T_{gas} combustion gases in contact with the surface (°R, K)

$T_{surface}$ tank temperature (°R, K)

α   radiation absorptivity

ε   radiation emissivity

σ   Stefan-Boltzmann constant (0.1713 x 10^{-8} Btu/ft^2 hr °R^4, 5.6704 x 10^{-8} W/m^2 K^4)

List of Figures

List of Tables

Bibliography

Anderson, C., Townsend, W., Zook, J., Cowgill, G., "The Effects of Fire Environment on a Rail Tank Car Filled with LPG", FRA-OR&D 75-31 (September, 1974)

API Standard 521, "Pressure-relieving and Depressuring Systems, Sixth Edition, January 2014

Birk, A.M., VanderSteen, J.D.J., Davison, C.R., Cunningham, M.H., Mirzazadeh, I., "PRV Field Trials – The Effects of Fire Conditions and PRV Blowdown on Propane Tank Survivability in a Fire", Transport Canada, TP 14045E (January 2003)

Birk, A.M., VanderSteen, J.D.J., "The Effect of Pressure Relief Valve Blowdown and Fire Conditions on the Thermo-Hydraulics within a Pressure Vessel", J. Pressure Vessel Tech., 128(2006), 467-475

DIERS, "Guidelines for Pressure Relief and Effluent Handling Systems" American Institute of Chemical Engineers Center for Chemical Process Safety, Wiley, New Jersey, 2nd edition, (2017)

Hendrickson, G.G., "Two-Phase Flow Considerations for Pressure Relief of Vessels Exposed to External Fires", DIERS Meeting Presentation, April 19, 2023

Melhem, G.A., "Part VI, Overtemperature Protection Consideration for Vessels Exposed to Fire", DIERS Meeting Presentation, July 19, 2021

Melhem, G.A., Croce, P.A., Abraham, H., "Data Summary of the National Fire Protection Association's BLEVE Tests", Process Safety Progress, 12(1993), 76-82

Melhem, G.A. and Gaydos, D., "Properly Calculate Vessel and Piping Wall Temperatures during Depressuring and Relief", Process Safety Progress, 34(2015), 64-71

Moodie, K., Cowley, L.T., Denny, R.B., Small, L.M., Williams, I., "Fire Engulfment Tests on a 5 Tonne LPG Tank", J. Hazard. Materials, 20(1988), 55-71

Melhem, G. A., "Reducing Uncertainty in LNG Fire Exposure Modeling", Paper Presented at the 2nd AIChE/CSChE LNG Topical Conference, Montreal – August 26, 2009

Melhem, G. A., H. Ozog, R. P. Stickles and Neil Prophet, "Effective Quantification of LNG Risks from Terminals and Floating Storage and Regasification Units (FSRU)", Paper Presented at the 2011 AIChE Spring Meeting, 7th Global Congress on Process Safety, Chicago, Illinois, March 13-16, 2011
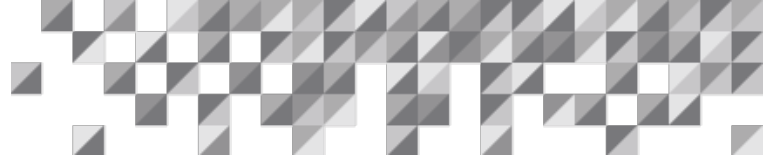
Melhem, G. A., "DIERS Technology Fundamentals. Part II – Runaway Reactions Characterization", AIChE VLS Webinar, January 20th, 2021